catalysts

MDPI

Article

g-C_3N_4 for Photocatalytic Degradation of Parabens: Precursors Influence, the Radiation Source and Simultaneous Ozonation Evaluation

Eryk Fernandes [1], Paweł Mazierski [2], Tomasz Klimczuk [3], Adriana Zaleska-Medynska [2], Rui C. Martins [1] and João Gomes [1,*]

[1] University of Coimbra, CIEPQPF—Chemical Engineering Processes and Forest Products Research Center, Department of Chemical Engineering, Faculty of Sciences and Technology, Rua Sílvio Lima, Polo II, 3030-790 Coimbra, Portugal
[2] Faculty of Chemistry, Department of Environmental Technology, University of Gdansk, Wita Stwosza 63, 80-308 Gdańsk, Poland
[3] Faculty of Applied Physics and Mathematics, Gdańsk University of Technology, 80-233 Gdańsk, Poland
* Correspondence: jgomes@eq.uc.pt; Tel.: +351-239798723; Fax: +351-239798700

Abstract: Graphitic carbon nitride (g-C_3N_4) is a promising catalyst for contaminants of emerging concern removal applications, especially as a visible-light-driven material. In this study, g-C_3N_4 catalysts were effectively synthesized through a simple thermal polymerization method, using melamine, urea, and thiourea as precursors to elucidate the influence of these compounds on the final product's photocatalytic performance. The degradation of a mixture of three parabens was investigated under different types of radiation: two artificial, ultraviolet-A (UVA) and visible LED, and natural sunlight. The urea-based catalyst (UCN) presented better results under all radiation sources, followed by thiourea, and finally, melamine. Among the artificial light sources, the degradation of parabens under UVA was considerably higher than visible—up to 51% and 21%, respectively—using UCN; however, the broader spectrum of natural sunlight was able to achieve the highest removals, up to 92%, using UCN. Comparing artificial radiation sources, UVA lamps presented 45% lower energy consumption and associated costs. Photocatalytic ozonation was tested using UCN and MCN, with UCN once more possessing superior performance and a synergetic effect between photocatalysis and ozonation, with complete removal under 12 min. The use of g-C_3N_4 was then successfully tested in initial screening and found to be an efficient alternative in more low-cost and feasible solar photocatalysis water treatment.

Keywords: catalysts synthesis; contaminants of emerging concern; graphitic carbon nitride; solar photocatalysis; ozonation

check for updates

Citation: Fernandes, E.; Mazierski, P.; Klimczuk, T.; Zaleska-Medynska, A.; Martins, R.C.; Gomes, J. g-C_3N_4 for Photocatalytic Degradation of Parabens: Precursors Influence, the Radiation Source and Simultaneous Ozonation Evaluation. *Catalysts* **2023**, *13*, 789. https://doi.org/10.3390/catal13050789

Academic Editors: Kangle Lv and Roberto Fiorenza

Received: 17 February 2023
Revised: 20 April 2023
Accepted: 21 April 2023
Published: 23 April 2023

Copyright: © 2023 by the authors. Licensee MDPI, Basel, Switzerland. This article is an open access article distributed under the terms and conditions of the Creative Commons Attribution (CC BY) license (https://creativecommons.org/licenses/by/4.0/).

1. Introduction

Water scarcity and contamination are currently one of the main global issues, affecting a larger population each year. At least 2 billion people lack access to safe drinking water sources, being exposed to multiple diseases, and around 2.3 billion people live in water-stressed locations, facing seasonal water shortages, of which more than 700 million live in high-risk areas [1]. In this context, population and industrial activity growth are directly responsible for the increase in the contamination of water sources, with multiple chemicals being unproperly disposed of or directed to inefficient treatment stations [2].

Contaminants of emerging concern (CECs) are a currently highly discussed group of pollutants, mostly due to the lack of information and general monitoring, along with their potential human and environmental health risks [3]. These chemicals, which comprise pesticides, hormones, industrial additives, pharmaceuticals, personal care products, and others—usually detected in ng L^{-1} and µg L^{-1}—are highly persistent, tending to accumulate in the environment, as typically found technologies in wastewater treatment plants

(WWTPs) are not capable of or can only partially degrade them. Parabens are a group of molecules among the CECs that are vastly used in pharmaceuticals and personal care products due to their preservative and antibacterial properties, becoming the focus of multiple studies and withdrawn from products due to their endocrine-disruptive characteristics and having been detected in tumorous tissues [4,5]. CECs have been found in multiple environments and locations, such as groundwater, soil, and atmosphere [2]. Therefore, efficient water treatment and reuse has become a necessary goal to enhance the quality and availability of this resource.

Various technologies have been investigated to achieve efficient and feasible alternatives for CECs elimination [6–8]. Among them, advanced oxidation processes (AOPs) appear as promising alternatives [8]. These techniques are based upon the generation of highly oxidative radicals, which possess the capacity to react with multiple pollutants efficiently and non-selectively. The main reactive species involved is hydroxyl radicals (·OH), but other species can also present important roles depending on the characteristics of molecules and may vary according to the specific process. Fenton (Fe/H_2O_2); photo-Fenton (Fe/H_2O_2/light); ozonation (O_3); persulfate ($S_2O_8^{2-}$); catalytic oxidation; photocatalysis (catalyst/light); and their multiple combinations and other alternatives compose the AOPs groups and have been extensively applied for the successful elimination of pollutants [7,9–12]. Different technologies in the AOPs group may possess more adequate features depending on the desired task.

Regarding parabens degradation, a variety of AOPs have been employed, such as Fenton, electro-Fenton, persulfate [13,14], and ozonation. Zúñiga-Benítez et al. [15], were able to remove up to 77% and 56% of methylparaben (MP) and ethylparaben (EP) in a mixture (C_i = 1 mg L^{-1}) with other benzophenones under 360 min using a solar photo-Fenton treatment. Solar photo–electro-Fenton, another variation of this AOP, has also been found to possess high efficiencies towards parabens abatement, with a complete removal under 180 min of methyl-, ethyl- and propylparaben (C_i = 0.30 mM), even when spiked in real secondary wastewater, as reported by Steter et al. [16]. Ozonation, which is already present in some water treatment facilities, was studied by Lee et al. [17], and completely removed 50 μg L^{-1} of methylparaben and its halogenated species present in mixtures in drinking water and wastewater effluents.

Photocatalysis has also been applied for the abatement of parabens and other CECs and encompasses a variety of photocatalytic materials that can be used. The photocatalytic reaction starts with the activation of the photo-responsive material, through photon irradiation, resulting in the excitation of an electron (e^-) from the valence band to the conduction band, leaving a positive hole. The band gap energy of the material is a determinant of the type of radiation needed for its activation.

The most used material is TiO_2, especially due to its optimized characteristics, high stability, photoactivity, low cost, and toxicity. However, the application of TiO_2 at larger scales may be compromised, as TiO_2 typically possesses large band gap energy, requiring a radiation source with higher energies and lower wavelengths, i.e., ultraviolet, which only comprises 4–6% of natural sunlight. Therefore, other materials have been intensely studied to reduce the process cost involved in the use of artificial and energy-consuming radiation sources.

Graphitic carbon nitride (g-C_3N_4) is currently a topic of high interest, particularly as it has simple synthesis methods and belongs to the group of visible-light-driven (VLD) materials. Thus, such materials may allow for the better use of natural solar radiation for its activation. As said, g-C_3N_4 synthesis is usually a simple process, as thermal polymerization is the main used route, using nitrogen- and carbon-rich compounds as precursors, which are typically abundant and have lower costs. As material synthesis does not require many different compounds and there is a variety of chemicals that can be applied, the study of different precursors is highly important for the optimization of g-C_3N_4 photocatalysis. The selected precursor may greatly affect important photocatalytic-related characteristics of the final catalyst, especially the specific surface area, the recombination rate of the

MOST WIEDZY Downloaded from mostwiedzy.pl

photogenerated species, and band gap energy. The usual hydrophobic layered morphology of g-C_3N_4 is known to possess a lower surface area and impede the electrons' mobility, increasing e^-/h^+ recombination, which decreases the material efficiency [18]. Thus, studies involving the adaptations and optimization of base properties are vital to obtain a more feasible product [19].

To overcome the common drawbacks of g-C_3N_4 and photocatalysis, the process can be further improved through its combination with ozone. Photocatalytic ozonation is a reaction that benefits from a boost in oxidative radicals' production due to the synergetic effect between both technologies. The catalyst can increase the decomposition of ozone in the solution, which possesses a typical low solubility in water, reducing the necessary ozone dose and associated costs. Meanwhile, ozone acts as an excellent electron acceptor, decreasing the recombination of photogenerated species. The application of g-C_3N_4 in photocatalytic ozonation studies is not yet widely explored, especially using more than simple structure molecules and matrices, but there has been some development in recent years [20–22].

Thus, this study aims to evaluate the use of g-C_3N_4 in the photocatalytic degradation of a mixture of methyl-, ethyl-, and propylparaben. The effect of different precursors in the final catalyst is assessed, using melamine, urea, and thiourea, as well as efficiency regarding their activation under different radiation sources (natural sunlight, ultraviolet-A (UVA), and visible light (LEDs)). The application of ozone and photocatalysis in combination is also verified on the mixture of parabens degradation improvement due to the synergetic effect of both technologies combined.

2. Results and Discussion

2.1. Catalysts Characterization

The different precursors applied for the synthesis of g-C_3N_4 were subjected to SDT analysis (Figure 1). This assessment enables comprehension of the decomposition profile of each chemical, establishing temperatures for the thermal polymerization synthesis and indicating possible intermediary substances and reactions.

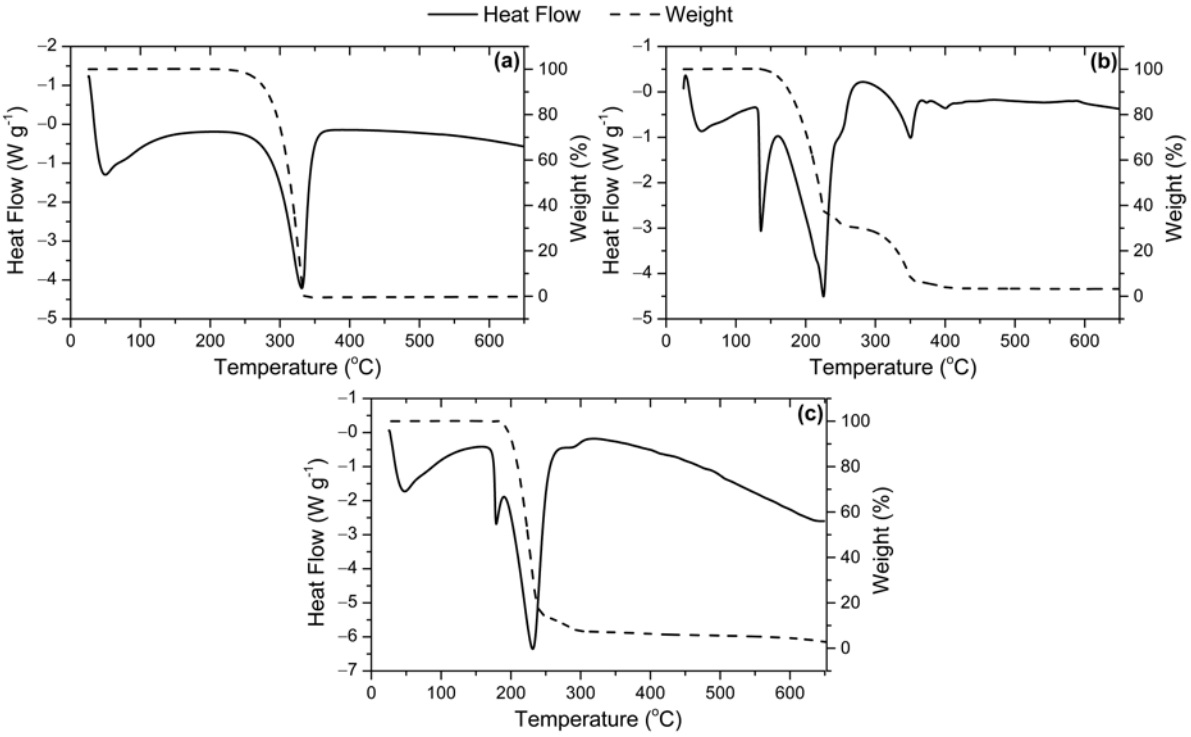

Figure 1. SDT analysis of (**a**) melamine, (**b**) urea, and (**c**) thiourea.

MOST WIEDZY Downloaded from mostwiedzy.pl

In the SDT results, a first endothermic peak, below 100 °C, is found in all heat flow curves, without any mass variation, which is mostly associated with the volatilization of the water, amino groups, and impurities content in each raw precursor. For melamine (Figure 1a), one major endothermic variation occurs at 331 °C, accompanied by significant weight loss, indicating the melting of melamine; the formation of different other molecules, such as melem and melam; and by-products, especially ammonia (NH_3), accounting for the weight loss (Figure 2) [23]. At this stage, melamine is arranged, leading to the formation of triazine and tri-s-triazine groups, which are the base structure of g-C_3N_4 [24,25].

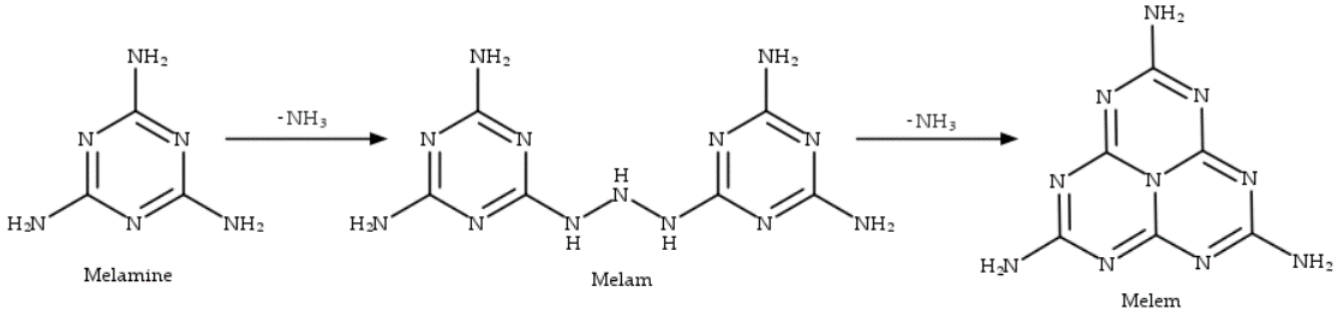

Figure 2. Melamine condensation into melam and melem at the beginning of g-C_3N_4 units' formation.

In the heat flow curve of the urea sample (Figure 1b), three important endothermic peaks were found. In the first peak, at 135.8 °C, occurs an obvious energetic disturbance with minimal mass variation, appointing a phase change of urea. Above 160 °C, the mass starts to decrease, possibly mostly due to the formation of ammonia and isocyanic acid (HNCO), as they exist mainly in the gas phase (Figure 3). From 160 °C and 225 °C, the second major endothermic peak, different intermediates are produced, most significantly biuret and isocyanuric acid (Figure 3) [23]. Between 225 °C and 350 °C, the ammonization and condensation of these molecules leads to the formation of ammelide, ammeline, and finally melamine, with the third endothermic peak at 350.3 °C; this is similar to the melamine SDT profile, which is associated with the melting of melamine and the consequent formation of the basic units of the g-C_3N_4 structure [26]. The thiourea results (Figure 1c) are similar to urea, differentiated by the higher melting point of thiourea at 179 °C and more abrupt and continuous weight loss, possibly due to the formation of heavier gaseous by-product, carbon disulfide (CS_2), and hydrogen sulfide (H_2S), compared to carbon dioxide (CO_2) and water (H_2O) [25].

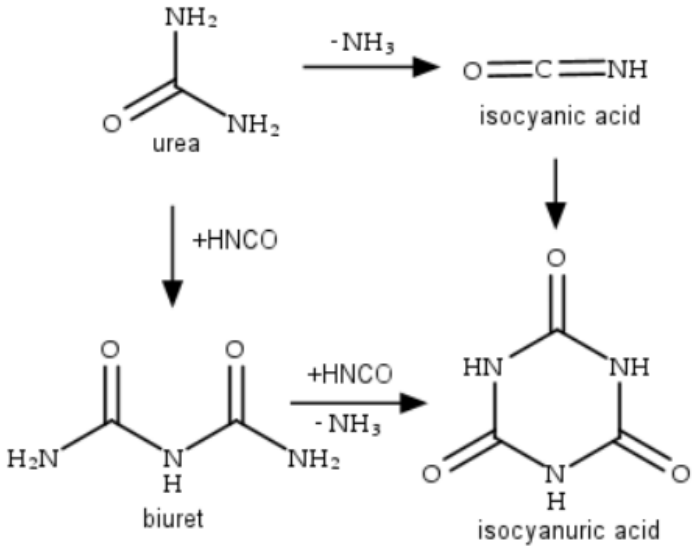

Figure 3. Possible intermediates formation through urea thermal decomposition.

Through the evaluation of the thermogravimetric analysis of the studied precursors, it is possible to determine that at the calcination temperature used, 550 °C, all the initial chemicals were completely converted.

Figure 4 presents the pXRD pattern of the g-C_3N_4 catalysts synthesized with different precursors. The presence of two main peaks originated from the graphite structure and tri-s-triazine units confirm the C_3N_4 structure in all synthesized samples. Reflections visible at 2θ = 13.1 and 27.2° are associated with the (100) and (002) planes, respectively [27,28]. The first peak is characteristic of the tri-s-triazine units while the second is related to the stacking of the aromatic system [28]. In all samples, between the above-mentioned peaks, two others can be observed, probably originating from decomposition or oxidation products formed during the thermal polymerization of C_3N_4 precursors [29]. Different peak intensities of the (002) plane can be attributed to defects related to varying degrees of polymerization, which is especially observed when using urea as a C_3N_4 precursor.

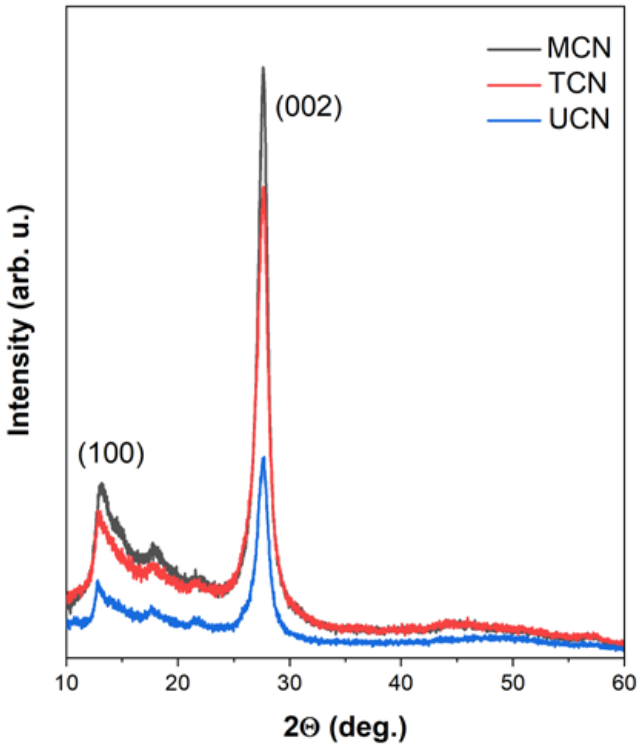

Figure 4. pXRD pattern of g-C_3N_4 catalysts synthesized with different precursors.

Surface morphology based on the HRSEM images of the g-C_3N_4 catalysts synthesized with different precursors is shown in Figure 5. In all samples, typical irregular plate-like structures can be observed; however, depending on the precursor type, the size of these plates differs. The smallest size was shown by the plates obtained using urea as a precursor, while the use of melamine as a C_3N_4 precursor resulted in large layers of blocks. The size of the plates obtained from urea was below 500 nm and had a thickness below 10 nm.

To determine the impact of precursor type on the surface properties, the BET surface area was determined using liquid nitrogen adsorption–desorption isotherms, as shown in Figure 6. The adsorption–desorption isotherm curves illustrated a type IV isotherm. The highest BET surface area reached the value of 82.52 m^2/g observed when urea was used as a C_3N_4 precursor, while the smallest BET surface area of 14.24 m^2/g was observed using melamine. The use of thiourea for synthesis made it possible to obtain a C_3N_4 material with a BET surface area of 21.38 m^2/g. The above-mentioned BET surface area values are consistent with the size of the plates observed in the SEM images, where the smallest plates obtained using urea as a precursor caused the highest BET surface area.

MOST WIEDZY Downloaded from mostwiedzy.pl

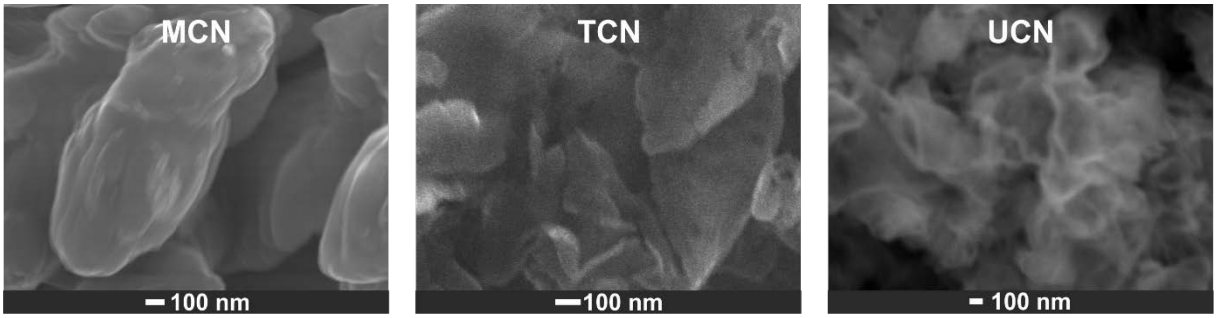

Figure 5. HRSEM images of g-C_3N_4 catalysts synthesized with different precursors.

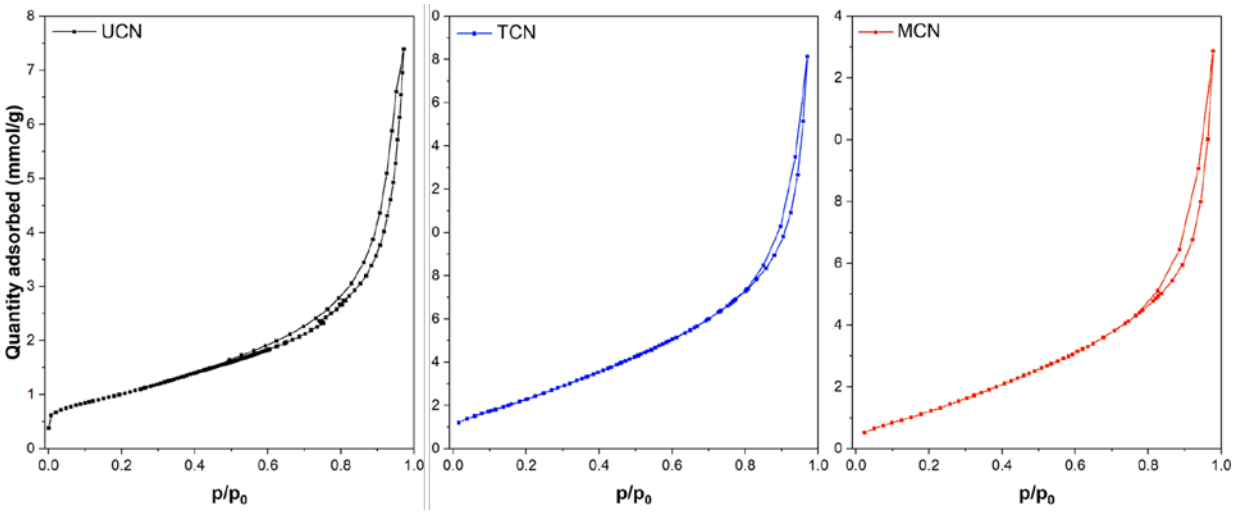

Figure 6. N_2 adsorption–desorption isotherm curves of g-C_3N_4 catalysts synthesized with different precursors.

The band gap energies of the three synthesized photocatalysts were estimated based on Tauc's plot, obtained through the UV-Vis DRS results (Figure 7). The final values of E_{bg} were 2.34, 2.60, and 2.66 eV for thiourea, melamine, and urea, respectively, taken as the interception of the tangents to the plots $(\alpha h\nu)^{1/2}$ versus $h\nu$.

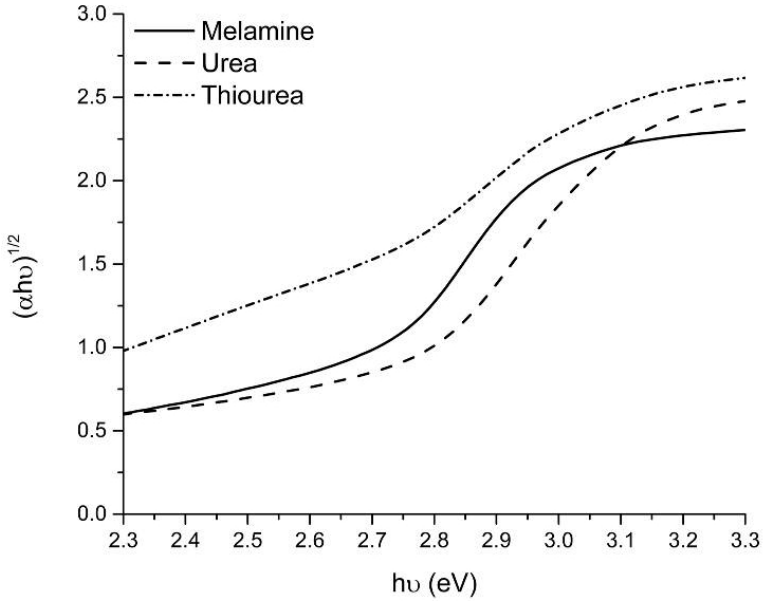

Figure 7. Tauc's plot of g-C_3N_4 using different precursors.

MOST WIEDZY Downloaded from mostwiedzy.pl

These variations may be associated with changes in the triazine and tri-s-triazine groups that form the g-C_3N_4 structure and are especially related to the electronic properties of the materials [23]. The insertion of foreign atoms within the structure of the catalysts, such as oxygen and thiourea, may also be responsible for the alterations in the optoelectronic properties [18]. Based on these results, the photocatalyst is expected to possess at least some absorption capacity of visible radiation; however, other intrinsic properties of each material may provide more significant influences over their photoactivity.

2.2. Photocatalytic Oxidation under Different Radiations

The efficiency of paraben elimination regarding the g-C_3N_4 catalysts synthesized with different precursors was initially tested under UVA radiation (Figure 8). Urea-based g-C_3N_4 (UCN) obtained the highest paraben removals, 50–52%, followed by thiourea (TCN), 33–36%, and finally melamine (MCN), 28–32%. The degradation of parabens tends to increase with the parallel increase in the alkyl chain length, due to the higher solubility and sites that may be more readily attacked by the radicals, making propylparaben degradation, for example, faster than the other employed contaminants.

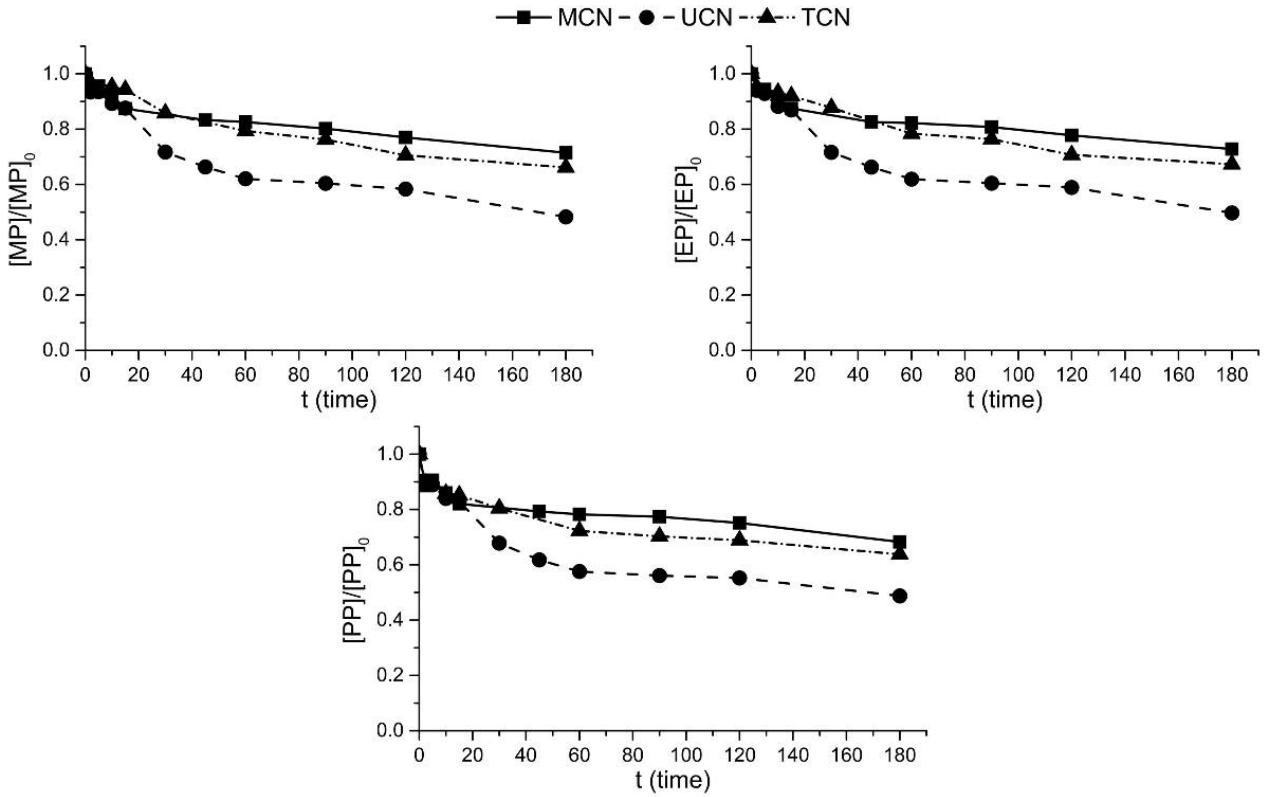

Figure 8. Methyl-, ethyl- and propylparaben degradation during photocatalytic oxidation under UVA radiation using melamine (MCN), urea (UCN), and thiourea (TCN)-based catalysts.

In the thermal condensation of thiourea and urea, as indicated previously, multiple gaseous by-products are formed (CO_2, H_2S, NH_3, CS_2). The produced bubbles of these related gases may then erupt and increase the specific surface areas of the final catalysts during polymerization [18]. The improved surface area allows a higher interaction between the materials with both the medium and contaminants, thus enhancing the production of radicals and abatement of pollutants. This mechanism is possibly responsible for the discovered BET surface areas.

Additionally, using urea as the catalyst precursor resulted in a powder with considerably lower density than the other materials, even following the same milling process. The lower density facilitates the dispersion of the material in the liquid, resulting in more

efficient light absorption and interaction with the medium. This fact may also compensate for the relatively higher band gap energy of urea g-C_3N_4 compared to the other precursors.

To better assess the elimination of parabens, a pseudo-first-order kinetics evaluation was conducted, as reported in other paraben oxidation studies, following Equation (1) [30,31]:

$$\ln\left(\frac{C}{C_0}\right) = kt \quad (1)$$

where k is the apparent reaction rate constant in min^{-1}.

The obtained data for methylparaben degradation under UVA radiation are plotted in Figure 9, and the remaining contaminants possessed similar profiles. During the data analysis, a distinct change was noted in the disposition of the results. After an initial higher reaction velocity, the degradation of parabens considerably decreases. This variation can be better translated as two linear equations, resulting then in two reaction rate constants, k_1, in a faster initial reaction phase, and k_2, where the slope obtained is lower. The reaction rate constants for each paraben are presented in Table 1.

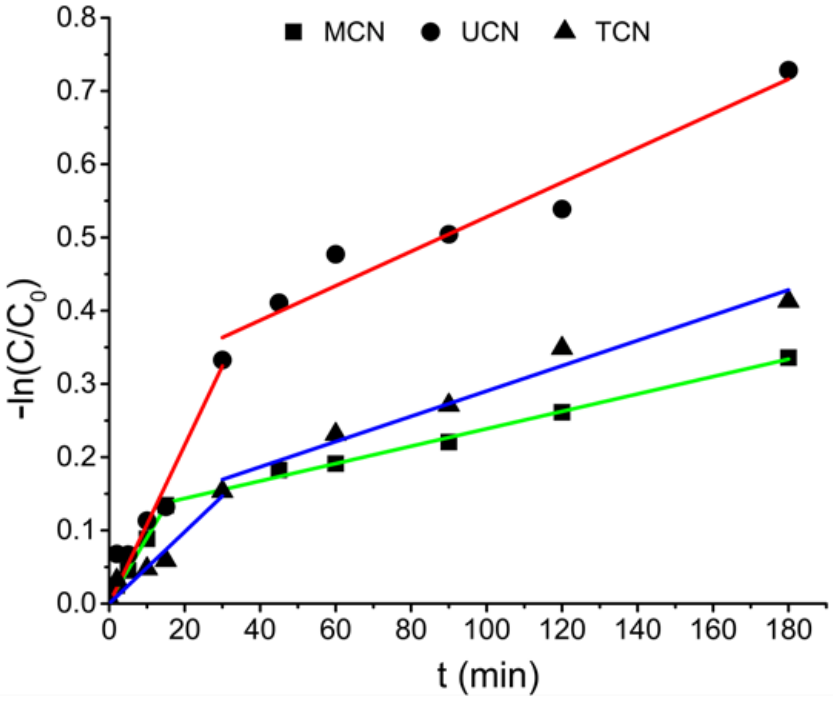

Figure 9. First-order kinetics of methylparaben degradation in UVA-assisted photocatalytic oxidation.

Table 1. Apparent reaction rate constants in UVA-assisted photocatalytic oxidation reactions for parabens degradation.

		$k_1 \times 10^{-3}$ (min)	$k_2 \times 10^{-3}$ (min)
MCN	**MP**	8.72	1.19
	EP	9.62	0.79
	PP	14.58	1.19
UCN	**MP**	10.82	2.35
	EP	9.87	1.94
	PP	11.79	1.56
TCN	**MP**	4.90	1.73
	EP	4.86	1.33
	PP	8.72	1.04

MOST WIEDZY Downloaded from mostwiedzy.pl

This change in the degradation profile may be associated with the presence of by-products in the medium. Even as the concentration of parabens decreases during the reaction, which would increase the availability of radicals, during their degradation multiple by-products can be formed [32]. These other molecules present in the medium may act as scavengers of the radicals, decreasing their interaction with the parabens and thus reducing their reaction rates.

Regarding the different catalysts, UCN possessed mostly higher reaction rate constants, especially k_2, which was at least 30% higher compared to the remaining catalysts, MCN and TCN. TCN presented lower rates, even with a slightly higher overall degradation of parabens; however, especially for MP and EP, the difference between k_1 and k_2 is smaller, resulting in a more balanced and uniform removal of contaminants. Propylparaben degradation rates were considerably higher compared to the other parabens, due to the already-appointed higher solubility and the number of sites available to be attacked by radicals.

To evaluate the photoactivity of g-C_3N_4 under higher wavelengths, LED strips were used as an artificial source of visible light. Paraben degradation profiles are presented in Figure 10. Following the same trend as discovered previously, the UCN catalyst resulted in higher depletion rates, followed by TCN and MCN.

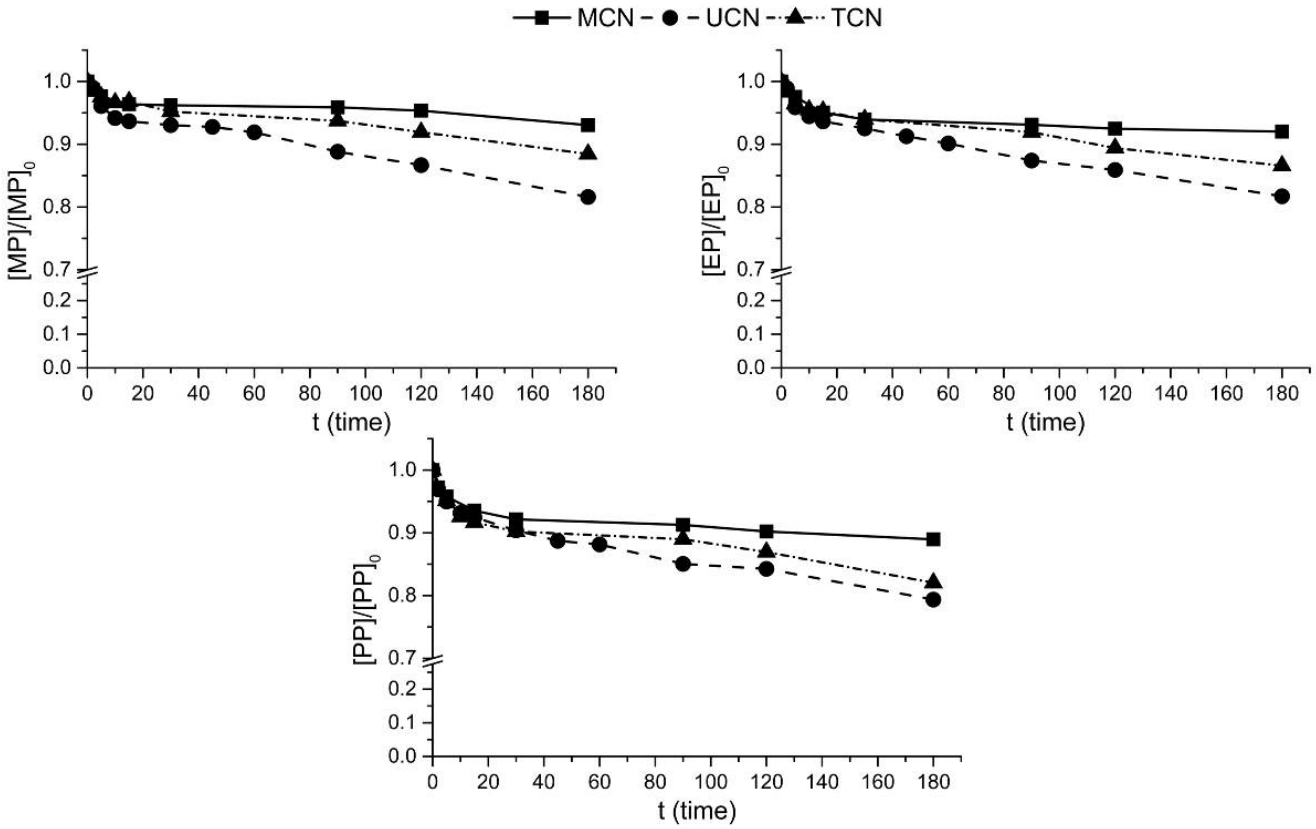

Figure 10. Methyl-, ethyl- and propylparaben degradation during photocatalytic oxidation under visible radiation using melamine (MCN), urea (UCN), and thiourea (TCN)-based catalysts.

Different from what was expected for known visible-light-driven materials, the photoactivity of all g-C_3N_4 was lower under visible radiation than UV, with the best result of 20.7% against a 51.3% removal of propylparaben using UCN under visible and UV radiation, respectively. Nonetheless, this indicates, even if in a lower amount, that synthesized catalyst can absorb a portion of wavelengths higher than 400 nm, which agrees with the estimated values of E_{bg}. The calculated reaction rate constants also corroborate the lower performance of all catalysts under visible radiation (Table 2). The variations of these

constants for the three catalysts and parabens are similar to the UVA results, confirming UCN's higher performance. TCN in this scenario possesses the second highest k_1 and k_2, as the difference between the overall parabens' degradation of MCN and TCN is also more evident.

Table 2. Apparent reaction rate constants in visible radiation photocatalytic oxidation reactions for parabens' degradation.

		$k_1 \times 10^{-3}$ (min)	$k_2 \times 10^{-3}$ (min)
MCN	**MP**	2.76	0.19
	EP	3.60	0.14
	PP	5.02	0.24
UCN	**MP**	5.09	0.91
	EP	5.05	0.82
	PP	6.24	0.84
TCN	**MP**	2.72	0.50
	EP	3.91	0.56
	PP	6.66	0.64

Graphitic carbon nitride catalysts are known to possess activity under visible light. However, some studies that compared these materials' activities under different wavelengths for contaminants removal have shown that UVA radiation can sometimes be more effective. Papailias et al. [33] obtained a 24% degradation of nitric oxide (NO) under UV irradiation against 14% when visible light was applied, using a melamine-based g-C_3N_4, even with the catalyst presenting a relatively lower band gap energy (2.76 eV). A possible explanation for this fact would be that the main peak regarding light absorption by the material could be situated near the transitional wavelengths between UVA and visible regions (<490 nm), while the used white LED strips mainly emit at 580–590 nm [34].

Several adaptations and increments can be made to boost the photocatalytic activity of g-C_3N_4 and the photocatalysis process overall. In fact, one of the main general advantages of g-C_3N_4 is its relatively simple production, which makes this material easily tunable. For example, during catalyst synthesis, templates can be used, or an exfoliation post-treatment can be added to improve the porosity and surface characteristics of the final product [35]. Other, more complex incorporations can also be conducted, such as doping and heterostructures formation, decreasing typical drawbacks such as the high recombination rates of the photogenerated species and electron mobility [36].

Finally, as one of the main purposes of this study, solar photocatalysis was evaluated for the contaminant's mixture treatment (Figure 11). A significant increase in process efficiency was achieved, especially regarding UCN and TCN. The urea-based catalyst once more achieved the highest efficiencies, with more than 92% elimination of each paraben, denoting an almost 40% increase in comparison to the UVA tests. TCN also presented an increased depletion of contaminants, up to 65%. The results obtained for the solar photocatalysis using MCN were highly similar to those found under UVA radiation, indicating that the catalyst produced through melamine thermal polymerization possesses a higher light absorption towards lower wavelengths. To ensure that the parabens' removal was due to the mechanisms involved in the photocatalytic reactions and produced radicals, a simple photolytic reaction was conducted in parallel. The concentration of contaminants during this experiment suffered no significant alterations (<5%), which confirms that the photocatalytic route is the main one responsible for parabens' elimination and agrees with other reports of solar-based treatments of parabens [37,38].

MOST WIEDZY Downloaded from mostwiedzy.pl

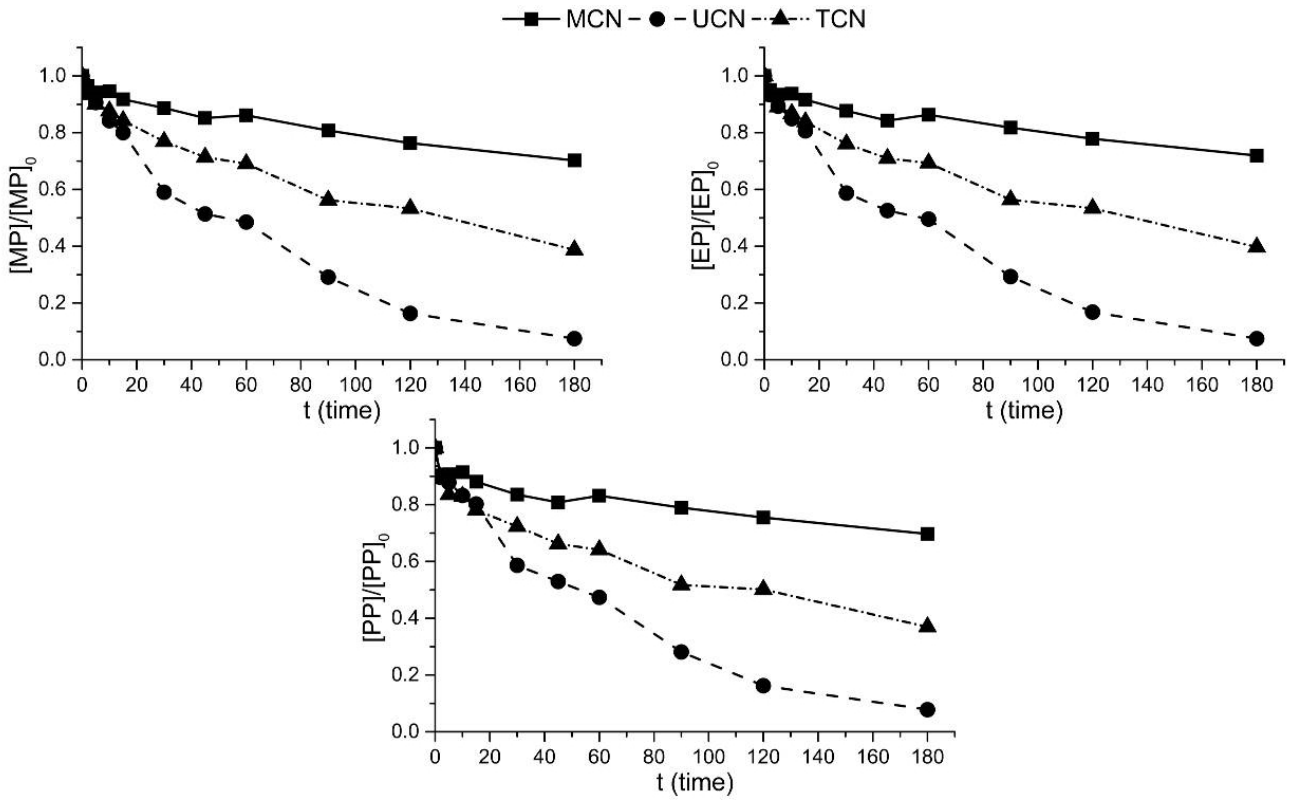

Figure 11. Methyl-, ethyl- and propylparaben degradation during photocatalytic oxidation under natural sunlight using melamine (MCN), urea (UCN), and thiourea (TCN)-based catalysts.

In contrast to the reactions under other radiation sources, the kinetic results of the solar photocatalytic reaction can be well adjusted ($R^2 > 0.96$) to a single linear regression (Figure 12). The disparity between the performance of the three catalysts becomes even more evident under natural sunlight, with UCN possessing an apparent reaction rate constant more than six and two times higher than MCN and TCN, respectively (Table 3).

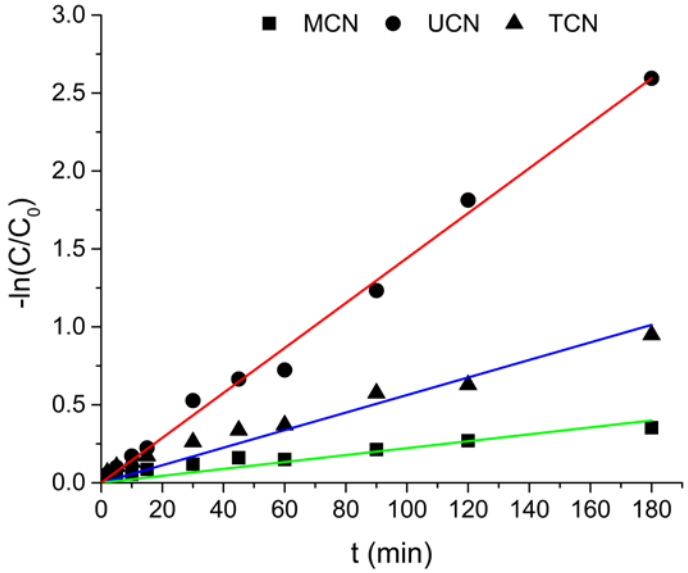

Figure 12. First-order kinetics of methylparaben degradation in sunlight-assisted photocatalytic oxidation.

MOST WIEDZY Downloaded from mostwiedzy.pl

Table 3. Apparent reaction rate constants in sunlight-assisted photocatalytic oxidation reactions for parabens' degradation.

		$k \times 10^{-3}$ (min)
MCN	**MP**	2.22
	EP	2.11
	PP	2.42
UCN	**MP**	14.41
	EP	14.32
	PP	14.36
TCN	**MP**	5.63
	EP	5.56
	PP	6.20

Additionally, an overall energy cost estimative (Table 4) related to the use of artificial radiation sources, UVA lamps, and visible LEDs was conducted regarding the studied catalyst with the best results—UCN. The LEDs possessed a 45% higher energy demand, although resulting in a considerably lower removal of parabens. This confirmed the lower performance of these materials under only visible radiation. The LEDs applied on the tests have a broader spectrum, which could be a possible explanation for their higher energy requirement and lower performance. The use of lamps with more specific wavelengths, especially at the beginning of the visible range (~400 nm), could provide better results.

Table 4. Energy requirement and costs associated with using artificial radiation sources for the photocatalytic degradation of the paraben's mixture using UCN.

Radiation Source	Contaminant	Removal (%)	E_{EO} (kWh m^{-3} $Order^{-1}$)	Energy Consumption (kWh m^{-3})	Cost (EUR m^{-3})
UVA	MP	51.7	4.91	27	6.4
	EP	50.3	4.89		
	PP	51.3	4.85		
Visible	MP	18.4	5.12	39	9.3
	EP	18.3	5.08		
	PP	20.6	5.04		

The electric energy per order (E_{EO}, kWh m^{-3} $order^{-1}$) was also calculated, using Equation (2), described by the electric energy needed to decrease a contaminant concentration by one order of magnitude in a specified volume of a contaminated solution [39]:

$$E_{EO} = \frac{P \cdot t \cdot 1000}{V \cdot \log\left({}^{C_i}/_{C_f}\right)} \quad (2)$$

where P is the input power in kW associated with the artificial radiation source; t is the treatment time in h; the factor 1000 converts g to kg; V is the treated volume in L; and C_i and C_f are the initial and final concentrations, respectively.

The E_{EO} is an important parameter to assess the overall energy consumption of a technology associated with its degradation performance. Dhaka et al. [40] calculated the E_{EO} for the degradation of ethylparaben (5 mg L^{-1}), in 100 mL solutions for 90 min, using different oxidants under UVC radiation: persulfate, hydrogen peroxide, and peroxymonosulfate, which were, respectively, 61.0, 68.7, and 143.7 kWh m^{-3}. Regarding photocatalysis, Mergenbayeva et al. [41] applied Ag_2CO_3 in UVA and visible (300–600 nm) photocatalysis of 5 mg L^{-1} of 4-tert-Butylphenol, a contaminant with an aromatic structure similar to parabens. In this study, E_{EO} of 9.1 and 8.3 kWh m^{-3} were found for the UVA and visible reactions, respectively.

MOST WIEDZY Downloaded from mostwiedzy.pl

The fact that solar irradiation can be so effective for g-C_3N_4 activation is crucial for the feasibility of the complete process. The energy requirement of artificial radiation sources can be one of the main expenses of photocatalytic treatment. Thus, as an inexpensive and efficient natural energy source, photo-activation using natural sunlight is a key aspect to achieve low-cost alternative treatment methods for CECs. The broad spectrum of wavelengths of solar irradiation is highly relevant for catalyst activation, as it possesses portions referring to ultraviolet, visible, and infrared radiation. The costs evaluated were singularly based on the energy consumption of the artificial radiation sources, and it is important to mention that other costs need to be accounted for in future, as well as more complex estimations—especially the costs associated with the reactor. These costs are expected to be higher for solar photo-reactors, as a greater area is often needed to achieve better performance.

Additionally, further investigation of different parameters is necessary to better identify the optimal conditions and provide additional knowledge regarding the characteristics of the intrinsic catalyst. The variations of catalyst concentration, the influence of reactor design, and different visible wavelength ranges, among others, deeply influence the overall performance and need to be optimized [42]. More specific parameters, such as the absorption and scattering of photons by the catalytic material, and the optical thickness, which can translate the overall effect of catalyst concentration and its optical properties, as well as their influence alongside the reactor geometry, are highly important for the scaling-up phase of photocatalytic systems, especially solar-based reactions [43,44].

2.3. Photocatalytic Ozonation

The UCN and MCN catalysts were then selected for evaluation in photocatalytic ozonation reactions, as they possessed the best and worst performances during previous tests. These materials were compared alongside single photolytic ozonation, in order to better understand their effect in this combination and possible synergetic effects (Figure 13).

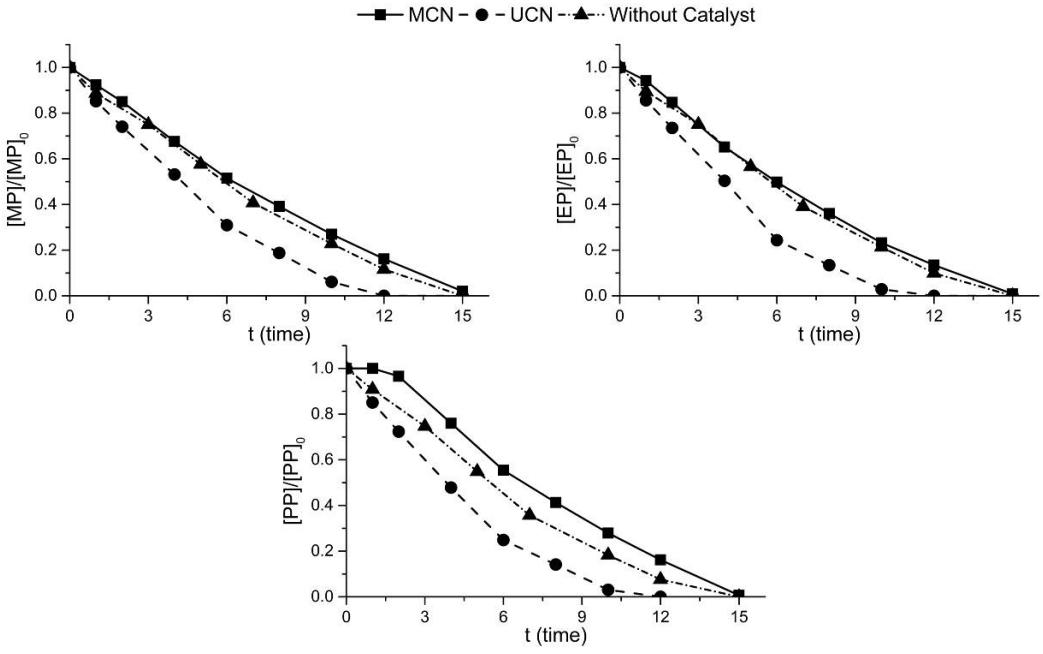

Figure 13. Methyl-, ethyl-, and propylparaben degradation during photolytic and photocatalytic ozonation under UVA radiation using melamine (MCN) and urea (UCN)-based catalysts.

The ozone-based processes were proved to greatly enhance paraben degradation, with a complete degradation under 15 min. Ozone is known to enable the fast degradation of parabens, as they possess highly electronic dense aromatic rings and ozone is a very efficient electron receptor.

MOST WIEDZY Downloaded from mostwiedzy.pl

Using a melamine-based catalyst provided no significative, or in the case of propylparaben, a negative effect over the pollutant's removal. Possibly in this reaction, the molecular ozone may possess a more significant role in the paraben's degradation than ·OH, and the ozone adsorption onto the catalyst surface, together with a higher mass transference resistance in the gas–liquid–solid medium, would decrease its availability to participate in such reaction [42].

By contrast, the use of urea as the catalyst precursor resulted in a better photocatalytic performance once more. As suggested in the photocatalytic oxidation tests, important characteristics of the g-C_3N_4 may be improved using urea. Once more, the formation of bubbles during the reaction and the overall benefits of urea that promote the higher specific surface area and porosity, in this case, not only increase the interactions between the catalyst and the liquid, but also facilitate the decomposition of ozone [18]. This higher interaction may also be associated with a decrease in the mass transference resistance, causing a faster production of radicals. This higher decomposition and the faster removal of parabens are also associated with a lower consumption of ozone, which can decrease the overall process cost, as ozone production is highly energy demanding.

Furthermore, the benefits of photocatalytic ozonation may be still increased in other scenarios. This combined process may be less selective in comparison to their individual technologies, which are of high interest in real water treatment conditions, providing a faster and higher degradation of complex contaminant mixtures and water matrices. Another factor that may differentiate ozonation and photocatalytic ozonation is the potential lower toxicity of the treated solution. Although single ozonation may eliminate contaminants in a faster way, especially electron-rich compounds such as parabens, partial oxidation is typically achieved, and it may lead to the formation of by-products that may be even more toxic than the initial contaminants [5]. Previous studies have shown that photocatalytic ozonation may lead preferentially to a mineralization route, producing only CO_2 and H_2O [6].

3. Materials and Methods

3.1. Chemicals

Methylparaben (MP), ethylparaben (EP), and propylparaben (PP) were obtained from Sigma-Aldrich (St. Louis, MO, USA). The paraben mixture solutions were prepared using ultrapure water and with a concentration of 1 mg L^{-1} of each paraben.

Melamine, urea, and thiourea were obtained from Sigma-Aldrich and used for the preparation of g-C_3N_4 catalysts. Methanol (99.9%, Honeywell, Charlotte, NC, USA) was applied for catalyst washing.

3.2. Catalysts Synthesis

The g-C_3N_4 was prepared following a thermal polymerization method [45]. Briefly, melamine (MCN), urea (UCN), and thiourea (TCN), used as precursors, were put in covered ceramic crucibles and placed in an oven for reaction. Polymerization occurred for 4 h at 550 °C, with a 5 °C min^{-1} rate. After cooling to room temperature, the samples were ground and washed using methanol, then dried at 60 °C for 12 h.

3.3. Photocatalytic and Ozonation Studies

In photocatalytic reactions under UVA radiation (λ = 365 nm), 3 lamps (Philips TL 6 W BLB, 16 mm, Amsterdam, the Netherlands) were used, while for visible radiation tests, a light emission diode (LED) strip, 26 W, was employed (λ = 580–590 nm) [34]. For solar photocatalysis, the information regarding solar radiation intensity was obtained from a near forecast station at Coimbra, Portugal (40.186622°, −8.4182372°). The catalyst load used in all reactions was 200 mg L^{-1}, which was previously optimized [42,46]. The concentration of each paraben in all reactions was 1 mg L^{-1}.

For the ozone-based reactions, an ozone generator (802N, BMT) was employed, producing ozone from a pure oxygen stream with the gas flow kept at 0.2 L min^{-1}.

MOST WIEDZY Downloaded from mostwiedzy.pl

3.4. Characterization Techniques

The thermal stability analysis of the precursors used was conducted using simultaneous differential scanning calorimetry (DSC)/thermogravimetric analysis (TGA), normally called simultaneous data thermal (SDT) analysis (Q600, TA Instruments, New Castle, DE, USA). The chemical samples were analyzed with a heating rate of 10 °C min^{-1}, under N_2 flow (100 mL min^{-1}) from 25 °C to 1200 °C.

The morphology of the obtained catalysts was evaluated by field-emission scanning electron microscopy (FE-SEM, JEOL JSM-7610F, Tokyo, Japan). Powder X-ray diffraction experiments were carried out at room temperature with a Bruker D8 Focus diffractometer (Billerica, MA, USA) with Cu Kα (λ = 1.54 Å) radiation and a LynxEye XE-T detector. A BET surface area analysis was performed on a Micro 200 (3P Instruments, Odelzhausen, Germany) at −196.2 °C. Before the measurements, the degassing of samples was performed with nitrogen gas at 200 °C for 5 h.

The band gap energy (E_{bg}) of the catalytic material was calculated using Tauc's plot, based on the optical absorption results obtained from UV-Vis diffuse reflectance spectra (DRS). The UV-Vis DRS spectra for carbon nitride-based catalysts were obtained using a Jasco V-650 spectrophotometer (Easton, MD, USA) for the wavelength range of 300 to 600 nm.

3.5. Analytical Analysis

For the contaminant concentration measurements, high-performance liquid chromatography (HPLC) (Alliance) was used. For the mobile phase, a 50/50 mixture of methanol and an acidic solution of 0.1% of orthophosphoric acid was used, at a flow rate of 1 mL min^{-1}. The sample volume injected was 100 µL and a C18 column was employed, kept at 40 °C. The paraben concentration was detected at 255 nm.

4. Conclusions

The synthesis of graphitic carbon nitride was successfully conducted using three different precursors (melamine, urea, and thiourea). The use of urea as a precursor produced a final catalyst with a higher surface area, and much smaller particles, as confirmed by SEM images, resulting in higher photocatalytic performance and interactions with the contaminants.

In all photocatalytic reaction tests under different radiation sources, the urea-based catalyst (UCN) presented the highest removal value. Solar photocatalysis, as a clean and cheap radiation source for wastewater treatment, proved to result in significantly higher efficiencies of removal, with up to 92% elimination in 180 min. The combination of photocatalysis and ozonation was demonstrated to be an excellent alternative to improve the system, achieving the complete removal of contaminants in under 12 min.

These results are an excellent first evaluation of the potential of g-C_3N_4 and demonstrate that this material can be applied in more feasible alternatives for the abatement of CECs. Additionally, its particular conditions can be further optimized to obtain a more efficient water treatment method.

Author Contributions: Conceptualization, E.F., J.G. and R.C.M.; methodology, E.F., P.M., T.K., A.Z.-M., J.G. and R.C.M.; investigation, E.F.; resources, P.M., T.K., A.Z.-M., J.G. and R.C.M.; writing—original draft preparation, E.F.; writing—review and editing P.M., A.Z.-M., J.G. and R.C.M.; visualization, E.F., P.M., T.K., A.Z.-M., J.G. and R.C.M.; supervision, J.G. and R.C.M.; funding acquisition, E.F., P.M., A.Z.-M., J.G. and R.C.M. All authors have read and agreed to the published version of the manuscript.

Funding: This work was financed by European Structural and Investment Funds through Portugal2020 by the project PhotoSupCatal—development of supported catalytic systems for wastewater treatment by photo-assisted processes (POCI-01-0247-FEDER-047545). The authors gratefully acknowledge FCT (Fundação para a Ciência e Tecnologia, Portugal) for the PhD grant (2020.06130.BD) and the financial support (CEECIND/01207/2018). Thanks are due to FCT/MCTES for the financial support to CIEPQPF (UIDB/00102/2020).

MOST WIEDZY Downloaded from mostwiedzy.pl

Data Availability Statement: Not applicable.

Conflicts of Interest: The authors declare no conflict of interest.

References

1. UN-Water. *Summary Progress Update 2021: SDG 6—Water and Sanitation for All*; UN-Water: Geneva, Switzerland, 2021.
2. Stefano, P.H.P.; Roisenberg, A.; Santos, M.R.; Dias, M.A.; Montagner, C.C. Unraveling the Occurrence of Contaminants of Emerging Concern in Groundwater from Urban Setting: A Combined Multidisciplinary Approach and Self-Organizing Maps. *Chemosphere* **2022**, *299*, 134395. [CrossRef]
3. Marson, E.O.; Paniagua, C.E.S.; Gomes Júnior, O.; Gonçalves, B.R.; Silva, V.M.; Ricardo, I.A.; Maria, M.C.; Amorim, C.C.; Trovó, A.G. A Review toward Contaminants of Emerging Concern in Brazil: Occurrence, Impact and Their Degradation by Advanced Oxidation Process in Aquatic Matrices. *Sci. Total Environ.* **2022**, *836*, 155605. [CrossRef] [PubMed]
4. Amin, M.M.; Tabatabaeian, M.; Chavoshani, A.; Amjadi, E.; Hashemi, M.; Ebrahimpour, K.; Klishadi, R.; Khazaei, S.; Mansourian, M. Paraben Content in Adjacent Normal-Malignant Breast Tissues from Women with Breast Cancer. *Biomed. Environ. Sci.* **2019**, *32*, 893–904. [CrossRef] [PubMed]
5. Jamal, A.; Rastkari, N.; Dehghaniathar, R.; Aghaei, M.; Nodehi, R.N.; Nasseri, S.; Kashani, H.; Yunesian, M. Prenatal Exposure to Parabens and Anthropometric Birth Outcomes: A Systematic Review. *Environ. Res.* **2019**, *173*, 419–431. [CrossRef]
6. Cantarella, M.; Gorrasi, G.; Di Mauro, A.; Scuderi, M.; Nicotra, G.; Fiorenza, R.; Scirè, S.; Scalisi, M.E.; Brundo, M.V.; Privitera, V.; et al. Mechanical Milling: A Sustainable Route to Induce Structural Transformations in MoS_2 for Applications in the Treatment of Contaminated Water. *Sci. Rep.* **2019**, *9*, 974. [CrossRef]
7. Yu, H.; Liu, Y.; Cong, S.; Xia, S.; Zou, D. Review of Mo-Based Materials in Heterogeneous Catalytic Oxidation for Wastewater Purification. *Sep. Purif. Technol.* **2023**, *312*, 123345. [CrossRef]
8. Feijoo, S.; Yu, X.; Kamali, M.; Appels, L.; Dewil, R. *Generation of Oxidative Radicals by Advanced Oxidation Processes (AOPs) in Wastewater Treatment: A Mechanistic, Environmental and Economic Review*; Springer: Dordrecht, The Netherlands, 2023; Volume 22, ISBN 0123456789.
9. Vaz, T.; Domingues, E.; Gomes, J.; Martins, R.C. Evaluation of the Activation Procedure on Oxone Efficiency for Synthetic Olive Mill Wastewater Treatment. *Catalysts* **2022**, *12*, 291. [CrossRef]
10. Loeb, S.K.; Alvarez, P.J.J.; Brame, J.A.; Cates, E.L.; Choi, W.; Crittenden, J.; Dionysiou, D.D.; Li, Q.; Li-Puma, G.; Quan, X.; et al. The Technology Horizon for Photocatalytic Water Treatment: Sunrise or Sunset? *Environ. Sci. Technol.* **2019**, *53*, 2937–2947. [CrossRef] [PubMed]
11. Hu, Q.; Zhang, M.; Xu, L.; Wang, S.; Yang, T.; Wu, M.; Lu, W.; Li, Y.; Yu, D. Unraveling Timescale-Dependent Fe-MOFs Crystal Evolution for Catalytic Ozonation Reactivity Modulation. *J. Hazard. Mater.* **2022**, *431*, 128575. [CrossRef]
12. Yang, T.; Yu, D.; Wang, D.; Yang, T.; Li, Z.; Wu, M.; Petru, M.; Crittenden, J. Accelerating Fe(III)/Fe(II) Cycle via Fe(II) Substitution for Enhancing Fenton-like Performance of Fe-MOFs. *Appl. Catal. B Environ.* **2021**, *286*, 119859. [CrossRef]
13. Ioannidi, A.; Frontistis, Z.; Mantzavinos, D. Destruction of Propyl Paraben by Persulfate Activated with UV-A Light Emitting Diodes. *J. Environ. Chem. Eng.* **2018**, *6*, 2992–2997. [CrossRef]
14. Chen, Y.; Deng, P.; Xie, P.; Shang, R.; Wang, Z.; Wang, S. Heat-Activated Persulfate Oxidation of Methyl- and Ethyl-Parabens: Effect, Kinetics, and Mechanism. *Chemosphere* **2017**, *168*, 1628–1636. [CrossRef]
15. Zúñiga-Benítez, H.; Muñoz-Calderón, A.; Peñuela, G.A. Removal of a Mix of Benzophenones and Parabens Using Solar Photo-Fenton and a Cylinder Parabolic Collector in Aqueous Solutions. *J. Environ. Chem. Eng.* **2018**, *6*, 7347–7357. [CrossRef]
16. Steter, J.R.; Brillas, E.; Sirés, I. Solar Photoelectro-Fenton Treatment of a Mixture of Parabens Spiked into Secondary Treated Wastewater Effluent at Low Input Current. *Appl. Catal. B Environ.* **2018**, *224*, 410–418. [CrossRef]
17. Lee, W.; Marcotullio, S.; Yeom, H.; Son, H.; Kim, T.H.; Lee, Y. Reaction Kinetics and Degradation Efficiency of Halogenated Methylparabens during Ozonation and UV/H_2O_2 Treatment of Drinking Water and Wastewater Effluent. *J. Hazard. Mater.* **2022**, *427*, 127878. [CrossRef] [PubMed]
18. Nguyen, T.K.A.; Pham, T.T.; Nguyen-Phu, H.; Shin, E.W. The Effect of Graphitic Carbon Nitride Precursors on the Photocatalytic Dye Degradation of Water-Dispersible Graphitic Carbon Nitride Photocatalysts. *Appl. Surf. Sci.* **2021**, *537*, 148027. [CrossRef]
19. Fernandes, E.; Gomes, J.; Martins, R.C. Semiconductors Application Forms and Doping Benefits to Wastewater Treatment: A Comparison of TiO_2, WO_3, and g-C_3N_4. *Catalysts* **2022**, *12*, 1218. [CrossRef]
20. Cao, H.; Wang, J.; Kim, J.H.; Guo, Z.; Xiao, J.; Yang, J.; Chang, J.; Shi, Y.; Xie, Y. Different Roles of Fe Atoms and Nanoparticles on g-C_3N_4 in Regulating the Reductive Activation of Ozone under Visible Light. *Appl. Catal. B Environ.* **2021**, *296*, 120362. [CrossRef]
21. Tan, Y.; Chen, W.; Liao, G.; Li, X.; Wang, J.; Tang, Y.; Li, L. Strategy for Improving Photocatalytic Ozonation Activity of g-C_3N_4 by Halogen Doping for Water Purification. *Appl. Catal. B Environ.* **2022**, *306*, 121133. [CrossRef]
22. Liao, G.; Zhu, D.; Li, L.; Lan, B. Enhanced Photocatalytic Ozonation of Organics by g-C_3N_4 under Visible Light Irradiation. *J. Hazard. Mater.* **2014**, *280*, 531–535. [CrossRef]
23. Su, Q.; Sun, J.; Wang, J.; Yang, Z.; Cheng, W.; Zhang, S. Urea-Derived Graphitic Carbon Nitride as an Efficient Heterogeneous Catalyst for CO_2 Conversion into Cyclic Carbonates. *Catal. Sci. Technol.* **2014**, *4*, 1556–1562. [CrossRef]

MOST WIEDZY Downloaded from mostwiedzy.pl

24. Zhao, Z.; Ma, Y.; Fan, J.; Xue, Y.; Chang, H.; Masubuchi, Y.; Yin, S. Synthesis of Graphitic Carbon Nitride from Different Precursors by Fractional Thermal Polymerization Method and Their Visible Light Induced Photocatalytic Activities. *J. Alloys Compd.* **2018**, *735*, 1297–1305. [CrossRef]
25. Alaghmandfard, A.; Ghandi, K. A Comprehensive Review of Graphitic Carbon Nitride (g-C_3N_4)–Metal Oxide-Based Nanocomposites: Potential for Photocatalysis and Sensing. *Nanomaterials* **2022**, *12*, 294. [CrossRef] [PubMed]
26. Gross, P.; Höppe, H.A. Biuret—A Crucial Reaction Intermediate for Understanding Urea Pyrolysis to Form Carbon Nitrides: Crystal-Structure Elucidation and In Situ Diffractometric, Vibrational and Thermal Characterisation. *Chem. A Eur. J.* **2020**, *26*, 14366–14376. [CrossRef]
27. Zhang, Y.; Pan, Q.; Chai, G.; Liang, M.; Dong, G.; Zhang, Q.; Qiu, J. Synthesis and Luminescence Mechanism of Multicolor-Emitting g-C_3N_4 Nanopowders by Low Temperature Thermal Condensation of Melamine. *Sci. Rep.* **2013**, *3*, 1943. [CrossRef]
28. Xin, G.; Meng, Y. Pyrolysis Synthesized g-C_3N_4 for Photocatalytic Degradation of Methylene Blue. *J. Chem.* **2013**, *2013*, 187912. [CrossRef]
29. Jiang, X.; Li, J.; Fang, J.; Gao, L.; Cai, W.; Li, X.; Xu, A.; Ruan, X. The Photocatalytic Performance of g-C_3N_4 from Melamine Hydrochloride for Dyes Degradation with Peroxymonosulfate. *J. Photochem. Photobiol. A Chem.* **2017**, *336*, 54–62. [CrossRef]
30. Petala, A.; Frontistis, Z.; Antonopoulou, M.; Konstantinou, I.; Kondarides, D.I.; Mantzavinos, D. Kinetics of Ethyl Paraben Degradation by Simulated Solar Radiation in the Presence of N-Doped TiO_2 Catalysts. *Water Res.* **2015**, *81*, 157–166. [CrossRef]
31. Álvarez, M.A.; Ruidíaz-Martínez, M.; Cruz-Quesada, G.; López-Ramón, M.V.; Rivera-Utrilla, J.; Sánchez-Polo, M.; Mota, A.J. Removal of Parabens from Water by UV-Driven Advanced Oxidation Processes. *Chem. Eng. J.* **2020**, *379*, 122334. [CrossRef]
32. Fernandes, E.; Martins, R.C.; Gomes, J. Photocatalytic Ozonation of Parabens Mixture Using 10% N-TiO_2 and the Effect of Water Matrix. *Sci. Total Environ.* **2020**, *718*, 137321. [CrossRef]
33. Papailias, I.; Giannakopoulou, T.; Todorova, N.; Demotikali, D.; Vaimakis, T.; Trapalis, C. Effect of Processing Temperature on Structure and Photocatalytic Properties of g-C_3N_4. *Appl. Surf. Sci.* **2015**, *358*, 278–286. [CrossRef]
34. Schachtner, J.; Bayer, P.; Von Wangelin, A.J. A Flow Reactor Setup for Photochemistry of Biphasic Gas/Liquid Reactions. *Beilstein J. Org. Chem.* **2016**, *12*, 1798–1811. [CrossRef]
35. Hassani, A.; Eghbali, P.; Metin, Ö. Sonocatalytic Removal of Methylene Blue from Water Solution by Cobalt Ferrite/Mesoporous Graphitic Carbon Nitride ($CoFe_2O_4$/Mpg-C_3N_4) Nanocomposites: Response Surface Methodology Approach. *Environ. Sci. Pollut. Res.* **2018**, *25*, 32140–32155. [CrossRef] [PubMed]
36. Rajeshwari, M.R.; Kokilavani, S.; Khan, S.S. Recent Developments in Architecturing the g-C_3N_4 Based Nanostructured Photocatalysts: Synthesis, Modifications and Applications in Water Treatment. *Chemosphere* **2021**, *291*, 132735. [CrossRef] [PubMed]
37. Moschogiannaki, M.; Frontistis, Z.; Kiriakidis, G.; Mantzavinos, D.; Binas, V. Porous Co_xNi_1-$XTiO_3$ Nanorods for Solar Photocatalytic Degradation of Ethyl Paraben. *J. Mater.* **2020**, *6*, 788–799. [CrossRef]
38. Peñas-Garzón, M.; Sampaio, M.J.; Wang, Y.L.; Bedia, J.; Rodriguez, J.J.; Belver, C.; Silva, C.G.; Faria, J.L. Solar Photocatalytic Degradation of Parabens Using UiO-66-NH_2. *Sep. Purif. Technol.* **2022**, *286*, 120467. [CrossRef]
39. Bolton, J.R.; Bircher, K.G.; Tumas, W.; Tolman, C.A. Figures-of-Merit for the Technical Development and Application of Advanced Oxidation Technologies for Both Electric- and Solar-Driven Systems. *Pure Appl. Chem.* **2001**, *73*, 627–637. [CrossRef]
40. Dhaka, S.; Kumar, R.; Lee, S.H.; Kurade, M.B.; Jeon, B.H. Degradation of Ethyl Paraben in Aqueous Medium Using Advanced Oxidation Processes: Efficiency Evaluation of UV-C Supported Oxidants. *J. Clean. Prod.* **2018**, *180*, 505–513. [CrossRef]
41. Mergenbayeva, S.; Atabaev, T.S.; Vakros, J.; Mantzavinos, D.; Poulopoulos, S.G. Photocatalytic Degradation of 4-Tert-Butylphenol Using Solar Light Responsive Ag_2CO_3. *Catalysts* **2022**, *12*, 1523. [CrossRef]
42. Fernandes, E.; Drosopoulou, S.; Mazierski, P.; Miodynska, M.; Gołaszewska, D.; Zaleska-Medynska, A.; Martins, R.C.; Gomes, J. Carbon Nitride Photoactivation Evaluation and Degradation of a Mixture of Parabens by Ozone Assistance. *J. Water Process Eng.* **2022**, *49*, 103018. [CrossRef]
43. Acosta-Herazo, R.; Mueses, M.Á.; Puma, G.L.; Machuca-Martínez, F. Impact of Photocatalyst Optical Properties on the Efficiency of Solar Photocatalytic Reactors Rationalized by the Concepts of Initial Rate of Photon Absorption (IRPA) Dimensionless Boundary Layer of Photon Absorption and Apparent Optical Thickness. *Chem. Eng. J.* **2019**, *356*, 839–849. [CrossRef]
44. Grčić, I.; Li Puma, G. Six-Flux Absorption-Scattering Models for Photocatalysis under Wide-Spectrum Irradiation Sources in Annular and Flat Reactors Using Catalysts with Different Optical Properties. *Appl. Catal. B Environ.* **2017**, *211*, 222–234. [CrossRef]
45. Miodyńska, M.; Mikolajczyk, A.; Mazierski, P.; Klimczuk, T.; Lisowski, W.; Trykowski, G.; Zaleska-Medynska, A. Lead-Free Bismuth-Based Perovskites Coupled with g-C_3N_4: A Machine Learning Based Novel Approach for Visible Light Induced Degradation of Pollutants. *Appl. Surf. Sci.* **2022**, *588*, 152921. [CrossRef]
46. Undergound, W. Solar Radiation Forecast. Available online: https://www.wunderground.com/dashboard/pws/ICOIMBRA41 (accessed on 3 June 2022).

Disclaimer/Publisher's Note: The statements, opinions and data contained in all publications are solely those of the individual author(s) and contributor(s) and not of MDPI and/or the editor(s). MDPI and/or the editor(s) disclaim responsibility for any injury to people or property resulting from any ideas, methods, instructions or products referred to in the content.

MOST WIEDZY Downloaded from mostwiedzy.pl